Electronic Supplementary Material (ESI) for Journal of Materials Chemistry A.

Supporting Information

Few-layer MoS_2 flakes as hole-selective layer for solution-processed hybrid organic hydrogen-evolving photocathodes

Sebastiano Bellani,[a†] Leyla Najafi,[a,b†] Andrea Capasso,[a] Antonio Esau Del Rio Castillo,[a] Maria Rosa Antognazza,[c] and Francesco Bonaccorso[a*]

[a] Graphene Labs, Istituto Italiano di Tecnologia, via Morego 30, 16163 Genova, Italy.

[b] Università degli studi di Genova, Dipartimento di Chimica e Chimica Industriale, Via Dodecaneso 31, 16163 Genova, Italy.

[c] Center for Nano Science and Technology @Polimi, Istituto Italiano di Tecnologia, Via Pascoli 70/3, 20133 Milano, Italy.

† These authors contributed equally

*E-mail: francesco.bonaccorso@iit.it

TEM analysis of the MoS_2 flakes

In Fig. 1a of the main text of the manuscript is reported a representative transmission electron microscopy (TEM) image of MoS_2 flakes, showing irregular shaped sheets with lateral size in the 30-800 nm range (mean value ~275 nm, *i.e*. mean area approx. 0.075 um^2) (see statistical analysis of the TEM images reported in Fig. 1B). Fig. S1 report additional TEM images to better illustrate the morphology of MoS_2 flakes evidenced by Fig. 1a.

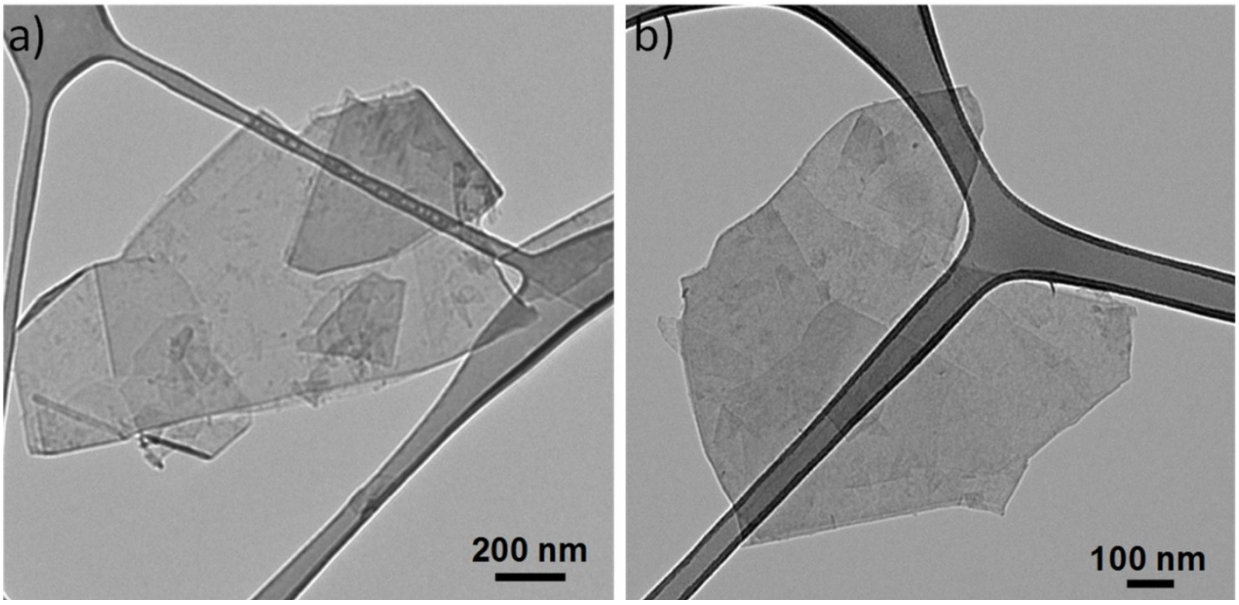

Fig. S1 a) and b) TEM image of the MoS_2 flakes deposited onto carbon coated Cu TEM grids.

AFM analysis of MoS_2 flakes

In Fig. 1c of the main text of the manuscript we show a representative AFM image of MoS_2 flakes with thickness of ~1.2 nm. Here, Fig. S2a shows an AFM image of MoS_2 flakes with thickness beetween 3 and 6 nm, while Fig. S2b shows an AFM image of a MoS_2 flake with a thickness up to 5.8 nm. Representative flakes' height profiles are shown in Fig. S2 by red lines.

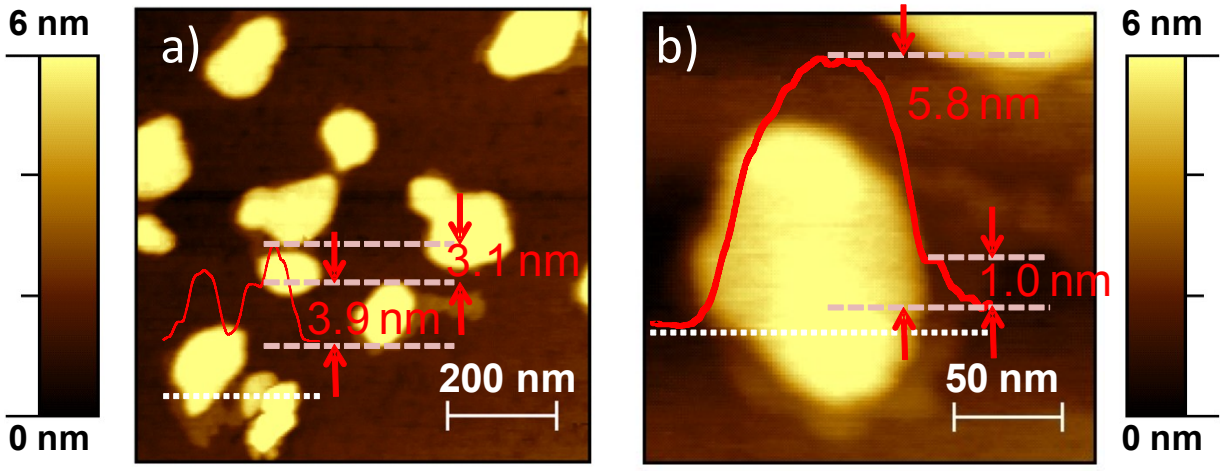

Fig. S2 a) AFM images of MoS_2 flakes deposited onto a V1-quality mica substrate, showing a multilayer structure (up to ~6 nm in thickness). b) AFM image on a zoomed part of image in panel a, showing an approx. 7-layers MoS_2 flake. The height profiles of representative flakes are also shown (red lines).

Statistical Raman analysis of the MoS_2 flakes

Fig. S3 reports the statistical Raman analysis of the MoS_2 flakes for the position, the full width at half maximum (FWHM) and the difference of the positions of the two main vibrational modes of MoS_2, i.e. E^1_{2g} and A_{1g}, while the Raman features of the bulk MoS_2 are summarized in Table S1. The $E^1_{2g}(\Gamma)$ mode of the MoS_2 flakes (located at ~380 cm^{-1}) exhibits softening with respect to the one of the bulk counterpart (located at 378 cm^{-1}), while no difference of the peak positon of the $A_{1g}(\Gamma)$ modes (~403 cm^{-1}) is observed. Thus, the frequency difference between $A_{1g}(\Gamma)$ and $E^1_{2g}(\Gamma)$ (24 cm^{-1}) of the MoS_2 decreases of ~2 cm^{-1} with respect to the bulk MoS_2 (26 cm^{-1}), see also Fig. 2b in the main text. The full width at half maximum (FWHM) of the $E^1_{2g}(\Gamma)$ and $A_{1g}(\Gamma)$ for the exfoliated MoS_2 increase of ~2 cm^{-1} and ~1 cm^{-1}, respectively, if compared with the corresponding modes of bulk MoS_2. As discussed in the main text of the manuscript, these results confirm the different topological structure of the MoS_2 flakes with respect to the bulk MoS_2.

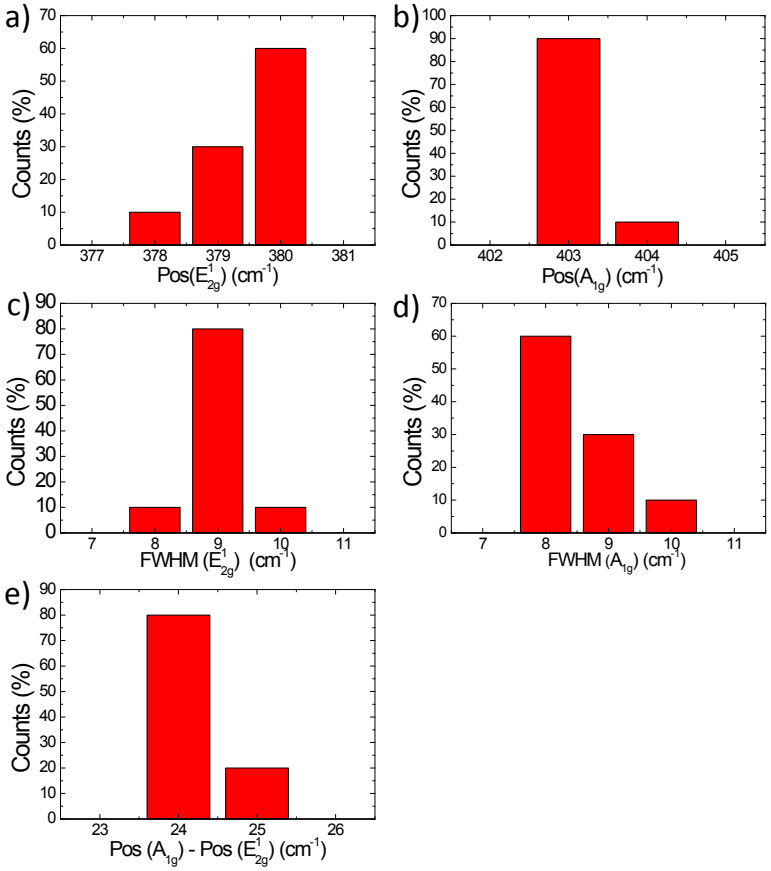

Fig. S3 Statistical Raman analysis of the MoS_2 flakes for a) the position of E^1_{2g} mode, b) the position of A_{1g} mode, c) the FWHM of the E^1_{2g} mode, d) FWHM of A_{1g} mode and e) the relative distance of the difference of the positions of the A_{1g} and E^1_{2g} modes (calculated on 30 different measurements). MoS_2 is deposited onto a Si wafer with 300 nm thermally grown SiO_2.

Table S1 Raman characteristics of bulk MoS_2.

POS(E^1_{2g})	FWHM(E^1_{2g})	POS(A_{1g})	FWHM(A_{1g})	POS(A_{1g})-POS(E^1_{2g})

378	7	403	7	26

AFM analysis of FTO/p-MoS_2 (10 mM)

Fig. S4 reports the AFM images for the FTO/p-MoS_2 (10 mM), which shows no differences in surface morphology with respect to the undoped case (FTO/MoS_2), whose image is shown in Fig. 3b of the main text. As shown in Table 2, the Ra of FTO/p-MoS_2 (10 mM) (Ra = 11.9 nm) has a similar value to that of FTO/MoS_2 (Ra = 11.6 nm). These data suggest that the p-doping treatment up to 10 mM does not affect the surface morphology of the deposited MoS_2 films. These results are in agreement with the SEM analysis of Fig. 4b-c of the main text of the manuscript.

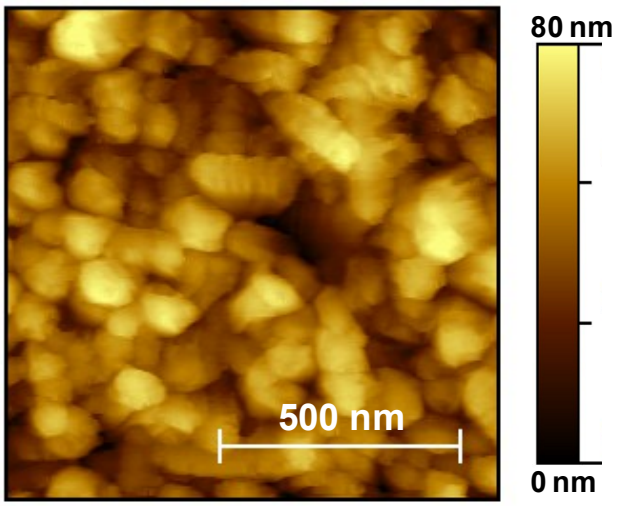

Fig. S4 AFM images of FTO/p-MoS_2 (10 mM). The MoS_2 films are deposited from a 0.1 mg mL^{-1} MoS_2 dispersion in IPA. The calculated roughness average (Ra) is 11.9 nm (see Table 2 in the main text of the manuscript).

Photoelectrochemical characterization of MoS_2-based photocathodes fabricated using different concentration of MoS_2 dispersion in IPA

Fig. S5 shows the photoelectrochemical responses of the MoS_2-based photocathodes fabricated using different concentration (0.05, 0.1, 0.4 mg mL^{-1}, dark cyan, orange and green lines) of MoS_2 dispersion in isopropanol (IPA) during the deposition of the MoS_2 films onto FTO. These results reveal that high photocurrent values are obtained for photocathodes with MoS_2 films obtained from 0.1 mg mL^{-1} concentration.

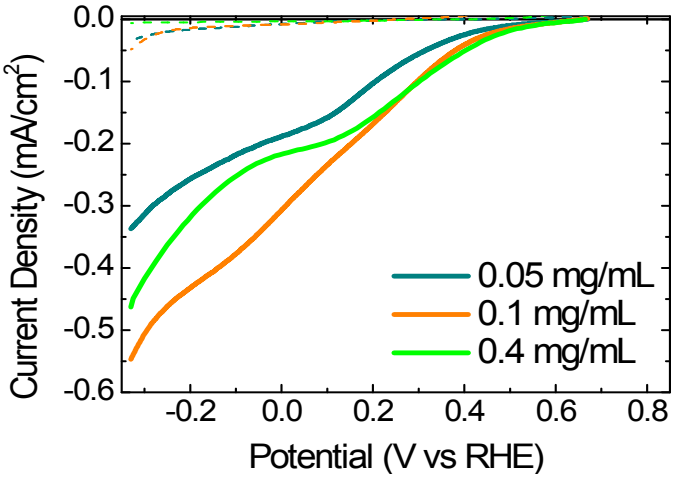

Fig. S5 linear sweep voltammetry measurements in 0.5 M H_2SO_4 solution at pH 1, under dark (dashed lines) and AM1.5 light illumination (100 mW cm^{-2}) (solid lines) for MoS_2-based photocathodes fabricated using different concentration (0.05, 0.1, 0.4 mg mL^{-1}, dark cyan, orange and green lines) of MoS_2 dispersion in IPA.

Photoelectrochemical characterization of p-MoS_2 (10 mM)-based photocathodes fabricated using different concentration of MoS_2 dispersion in IPA

Fig. S6 shows the photoelectrochemical responses of the p-MoS_2 (10 mM)-based photocathodes fabricated using different concentration (0.05, 0.1, 0.4 mg mL^{-1}, cyan, red and yellow lines) of MoS_2 dispersion in IPA for the deposition of the MoS_2 films onto FTO. As for the undoped MoS_2-based photocathodes (see Fig. S5), these results reveal that high photocurrent values are obtained for photocathodes with MoS_2 films obtained from 0.1 mg mL^{-1} concentration, whose analysis is reported in the main text of the manuscript.

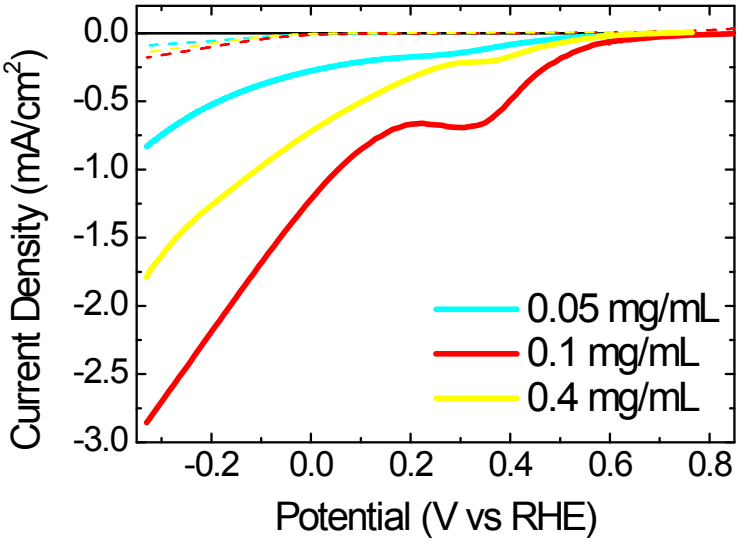

Fig. S6 Linear sweep voltammetry measured in 0.5 M H_2SO_4 solution at pH 1, under dark (dashed lines) and AM1.5 light illumination (100 mW cm^{-2}) (solid lines) for p-MoS_2 (10 mM)-based photocathodes fabricated using different concentration (0.05, 0.1, 0.4 mg mL^{-1}, cyan, red and yellow lines) of MoS_2 dispersion in IPA.

Linear sweep voltammetry (LSV) measurements of FTO/MoS_3

Fig. S7 reports two consecutive LSVs of FTO/MoS_3 measured in 0.5 M H_2SO_4 solution at pH 1, which is the same testing conditions of the LSVs reported in Fig. 6 for the photocathodes studied in this work. It is evident that the first LSV exhibits a broad reduction peak (marked by dashed blue oval) at positive potentials with respect to the HER (located at ~-0.2 V *vs.* RHE). The peak is reduced during the second LSV, which also shows a shift of the HER activity towards more positive potentials, as indicated by the blue arrow (see also the inset panel where LSV scan are showed over a negatively extended range of potential). These results confirm that during the first LSV scans the MoS_3 is reduced towards more catalytic MoS_{2+x} species, as also studied by other works (see ref. 68(b) of the main manuscript).

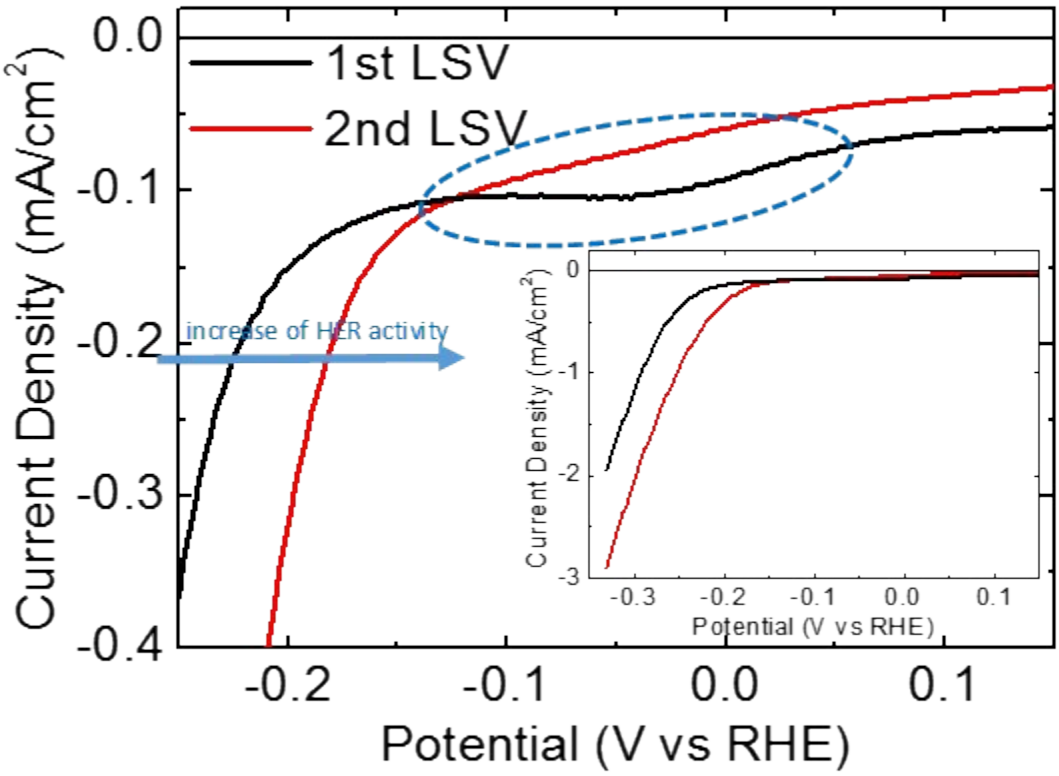

Fig. S7 Consecutive LSVs of FTO/MoS_3 measured in 0.5 M H_2SO_4 solution at pH 1. The broad reduction peak at potentials more positive than the HER (located at ~-0.2 V *vs.* RHE) is marked dashed blue oval and it is more pronounced during the first LSV. The peak is reduced during the second LSV, which also shows a shift of the HER activity (as evidenced by the blue arrow). The inset panel show the same LSVs of the main panel, extended over larger J and V scales.

Cyclic Voltammetry measurements on MoS_2 films

Fig. S8 reports Moreover, cyclic voltammetry (CV) measurements of MoS_2 films deposited on glassy carbon (GC) substrates by consequent drop casting steps from 0.4 mg mL^{-1} MoS_2 dispersion in IPA until reaching a loading of MoS_2 of 0.5 mg cm^{-1}. The figure also reports the CV of GC as reference background, revealing its electrochemical inertness. These data show the absence of irreversible redox reaction involving MoS_2 films under the HER-working condition of the photocathodes reported in Fig. 6 of the main text of the manuscript, in agreement with the electrochemical stability of the MoS_2 expressed in several energy conversion and storage devices, including fuel and water splitting cells, batteries and supercapacitors (see ref. 70-73 in the main text of the manuscript). In the inset to Fig. S8 the HER-electrocatalytic activity of the MoS_2 is also reported by LSV measurement over more negative voltages (up to -0.8 V vs RHE), showing onset over-potential of ~200 mV with respect to the RHE potential, in accordance with previous studies on layered MoS_2 materials (see ref. 71 in the main test of the manuscript). It is worth to note that this value is similar to that obtained for the MoS_3 (180 mV) (see Fig. 6 in the main text) used as EC in the photocathodes here studied, suggesting its possible exploitation in the photocathodes' structures as well as EC.

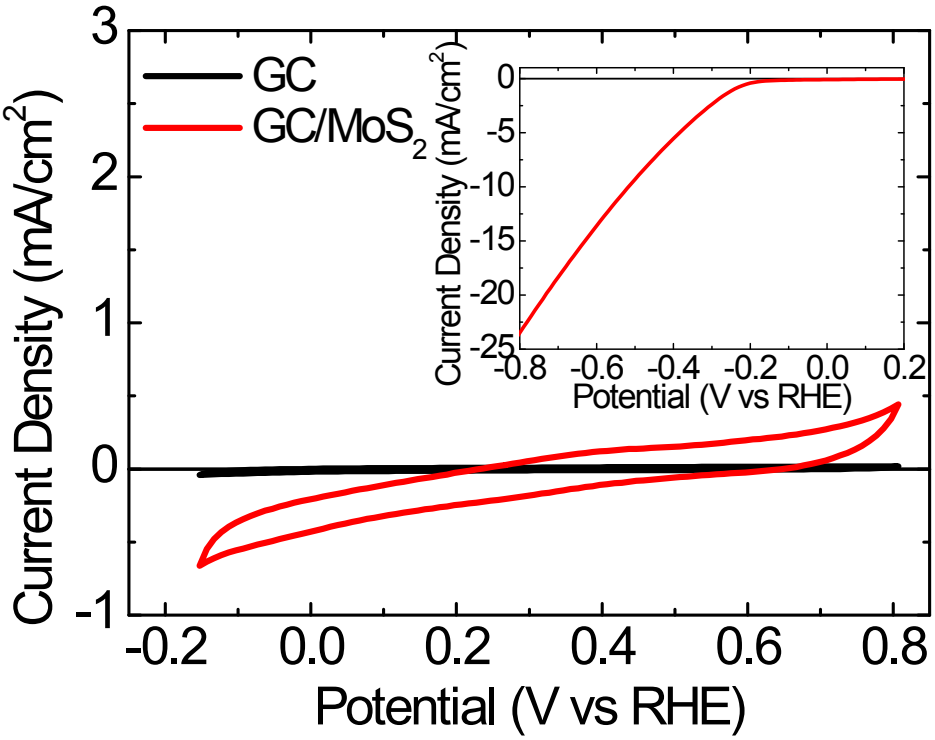

Fig. S8 CVs measured for GC and GC/MoS_2 samples in in 0.5 M H_2SO_4 solution at pH 1. Voltage scan rate: 500 mV s^{-1}. MoS_2 films are deposited on glassy carbon (GC) substrates by consequent drop casting steps from 0.4 mg mL^{-1} MoS_2 dispersion in IPA until reaching a loading of MoS_2 of 0.5 mg cm^{-1}. The inset panel show the HER-electrocatalytic activity of MoS_2 flakes, as measured by LSV on GC/MoS_2 sample.

References

1 C. Lee, H. Yan, L. E. Brus, T. F. Heinz, J. Hone and S. Ryu, ACS Nano, 2010, **4**, 2695.